ACS NANO

www.acsnano.org

ARTICLE

Giant Anisotropic Magnetoresistance in Few-Layer α-$RuCl_3$ Tunnel Junctions

Mathieu Massicotte,* Sam Dehlavi, Xiaoyu Liu, James L. Hart, Elio Garnaoui, Paula Lampen-Kelley, Jiaqiang Yan, David G. Mandrus, Stephen E. Nagler, Kenji Watanabe, Takashi Taniguchi, Bertrand Reulet, Judy J. Cha, Hae-Young Kee, and Jeffrey A. Quilliam

Cite This: https://doi.org/10.1021/acsnano.4c06937

Read Online

ACCESS | Metrics & More | Article Recommendations | Supporting Information

ABSTRACT: The spin−orbit-assisted Mott insulator α-$RuCl_3$ is proximate to the coveted quantum spin liquid (QSL) predicted by the Kitaev model. In the search for the pure Kitaev QSL, reducing the dimensionality of this frustrated magnet by exfoliation has been proposed as a way to enhance magnetic fluctuations and Kitaev interactions. Here, we perform angle-dependent tunneling magnetoresistance (TMR) measurements on ultrathin α-$RuCl_3$ crystals with various layer numbers to probe their magnetic, electronic, and crystal structures. We observe a giant change in resistance, as large as ∼2500%, when the magnetic field rotates either within or out of the α-$RuCl_3$ plane, a manifestation of the strongly anisotropic spin interactions in this material. In combination with scanning transmission electron microscopy, this tunneling anisotropic magnetoresistance (TAMR) reveals that few-layer α-$RuCl_3$ crystals remain in the high-temperature monoclinic phase at low temperatures. It also shows the presence of a zigzag antiferromagnetic order below the critical temperature $T_N \simeq 14$ K, which is twice the one typically observed in bulk samples with rhombohedral stacking. Our work offers valuable insights into the relation between the stacking order and magnetic properties of this material, which helps lay the groundwork for creating and electrically probing exotic magnetic phases such as QSLs via van der Waals engineering.

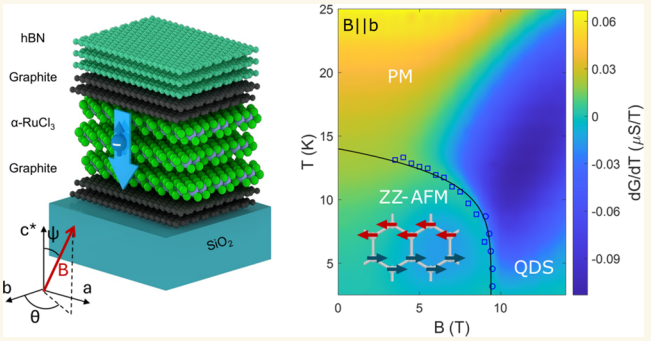

KEYWORDS: *magnetic 2D materials, α-$RuCl_3$, anisotropic magnetoresistance, tunnel junctions, spintronics, magnetic phase diagram*

INTRODUCTION

The quantum spin liquid (QSL) is an elusive state of matter in which quantum fluctuations and magnetic frustration generate long-range quantum entanglement and prevent magnetic ordering down to zero temperature.[1−3] One prominent type of QSLis predicted by the exactly solvable Kitaev model.[4] The Kitaev QSL has two varieties of fractional excitation, Majorana Fermions and fluxes, as its elementary excitations. The unusual quantum statistics of these excitations make it promising for topological quantum computation.[5] It was later shown that this model could be materialized in spin−orbit-assisted Mott insulators with bond-dependent Ising interactions.[6,7] The ensuing search for candidate Kitaev materials led to the emergence of α-$RuCl_3$, a van der Waals material, as one of the main prospects.[8−11] Despite early studies reporting an unconventional continuum of magnetic excitations,[12−14] α-$RuCl_3$ presents a zigzag antiferromagnetic (AFM) ground state, which preempts the realization of a pure QSL ground state. Nevertheless, this magnetic order can be quenched by applying an in-plane magnetic field larger than a critical field B_c, typically on the order of 6−8 T.[15−19] The report of half-integer quantization of the thermal Hall conductance just above this critical field generated huge interest, as it provided strong evidence of a Kitaev QSL phase in this field regime.[20] Yet, because of reproducibility issues caused by sample variations,[21−23] other approaches are currently being explored to suppress magnetic order and enhance Kitaev interaction in α-$RuCl_3$.

A tantalizing route to realizing a true Kitaev QSL in α-$RuCl_3$ is to reduce its dimensionality via mechanical exfoliation in order to enhance order parameter fluctuations. Raman

Received: May 24, 2024
Revised: August 18, 2024
Accepted: August 19, 2024

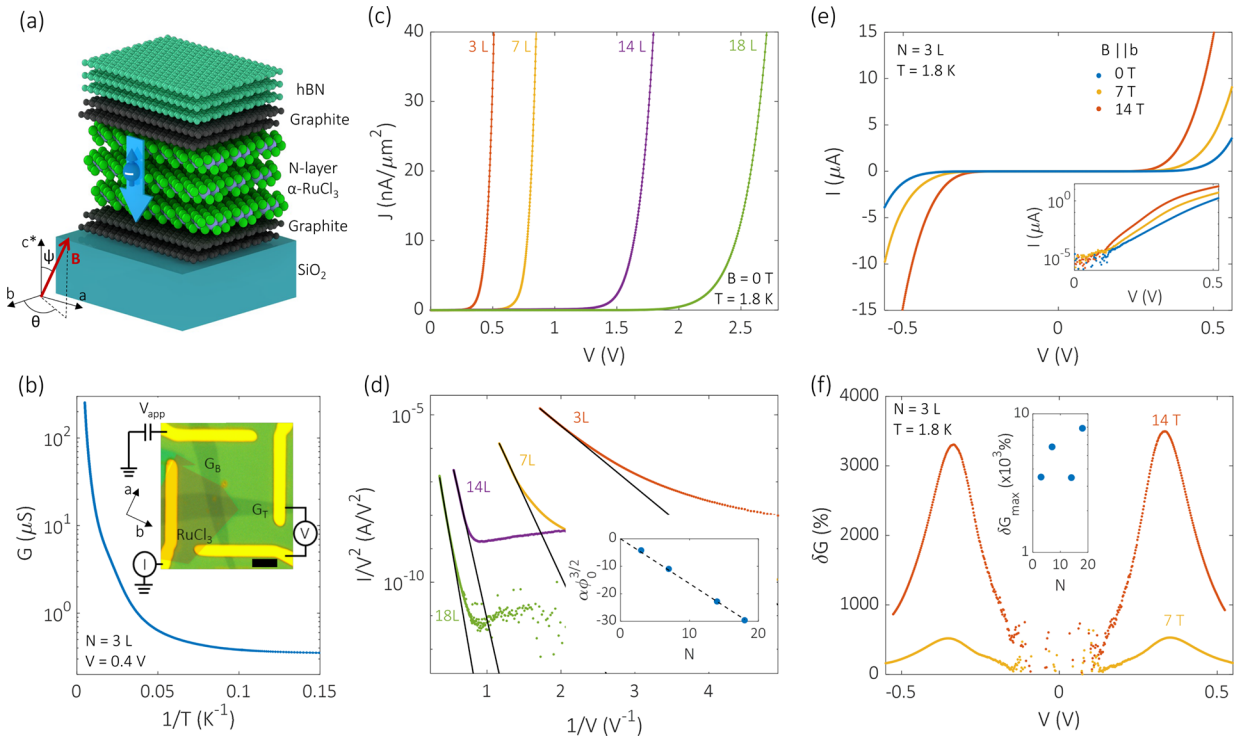

Figure 1. Graphite/ α-$RuCl_3$/graphite MTJs. (a) Schematic representation of electron tunneling in a van der Waals heterostructure under an external magnetic field B (red arrow). The heterostructure comprises two graphite sheets separated by an α-$RuCl_3$ barrier with N = 3 layers. It is covered by a flake of hBN and deposited on a SiO_2/Si substrate. The direction of the B field is defined by azimuthal angle ψ and polar angle θ. (b) Temperature dependence of conductance G of the trilayer device (N = 3) at zero field and V = 0.4 V. Inset: Optical image of a trilayer MTJ. α-$RuCl_3$ is colored orange for clarity. The top (G_T) and bottom (G_B) graphite are deposited on top of the Au/Ti contacts. V_{app} represents the voltage applied to the lead while V is the voltage measured across the junction. The scale bar is 10 μm. (c) Current density J = I/A (A is the area of the junction) as a function of V for MTJs with various numbers N of the α-$RuCl_3$ layer at zero field and 1.8 K. (d) Plot of $\ln(I/V^2)$ as a function of $1/V$ for the same measurement as in (c). The black lines are linear fits corresponding to the FN tunneling model. Inset: $\alpha\phi_0^{3/2}$ vs N. The blue points are obtained from the fits shown in the main panel, while the dashed line is a linear fit to the data. (e) Current I as a function of V measured at 1.8 K in a trilayer device under various values of the B field pointing along the b axis (see the inset of b). Inset: Same data on a semilog scale. (f) Magnetoconductance δG of the trilayer device as a function of V for B = 7 and 14 T. The maximum indicates the onset of the FN tunneling regime. Inset: The maximum magnetoconductance was measured at B = 14 T in devices with different layer numbers N.

spectroscopy studies reported robust magnetic fluctuations down to the monolayer as well as the presence of lattice distortions,[24−26] which were also observed by low-energy electron diffraction measurements.[27] Such mechanical strain may alter the magnetic phase of the monolayer, as suggested by *ab initio* calculations.[28] Recent tunneling studies also reported these distortions[29] and found that they can lead to a reversal of the magnetic anisotropy to easy-axis anisotropy for monolayer samples.[30] Furthermore, the van der Waals nature of α-$RuCl_3$ allows for the manipulation and investigation of its magnetic state by coupling it to other two-dimensional (2D) materials. Electronic transport and optical studies on α-$RuCl_3$/graphene heterostructures reported a large charge transfer between the two layers,[31−34] in agreement with first-principles calculations.[35−37] Transport measurements on these heterostructures also revealed proximity effects at low temperatures, hinting at the presence of an ordered magnetic ground state in exfoliated α-$RuCl_3$ crystals.[26,32] However, the magnetic and crystal structures of these flakes remain mostly unknown. In particular, the relation between the stacking order and magnetic properties of this material remains poorly understood, even for bulk crystals.[21]

Here, we investigate the magnetic and crystal structure of few-layer α-$RuCl_3$ flakes by measuring their angle-dependent tunneling magnetoresistance (TMR) (Figure 1a). This device-oriented technique, which has proven successful in studying other 2D magnets,[30,38−48] provides a sensitive and versatile tool to probe magnetism in nanoscale materials. Unlike other 2D materials, we observe a giant anisotropy of the TMR in α-$RuCl_3$. This effect enables us to track the magnetic phase diagram and magnetocrystalline anisotropy of α-$RuCl_3$ flakes with thicknesses ranging from 3 to 18 layers. Our results indicate that they host an AFM ground state with enhanced critical field and temperature compared to most bulk samples, and have a monoclinic crystal structure, which is supported by a high-resolution scanning transmission microscopy (STEM) study of isolated flakes. We use this knowledge to calculate the electronic structure of few-layer α-$RuCl_3$ and quantitatively explain our TMR measurements.

RESULTS

Transport in Graphite/α-$RuCl_3$/Graphite Heterostructures. Our magnetic tunnel junctions (MTJ) are made by placing an exfoliated α-$RuCl_3$ flake between two graphite flakes, capped by a crystal of hBN (see Methods and Supporting Information, Figure S1 for details on device fabrication). The graphite contacts are arranged in a cross geometry, allowing for precise four-probe measurements of the

https://doi.org/10.1021/acsnano.4c06937
ACS Nano XXXX, XXX, XXX−XXX

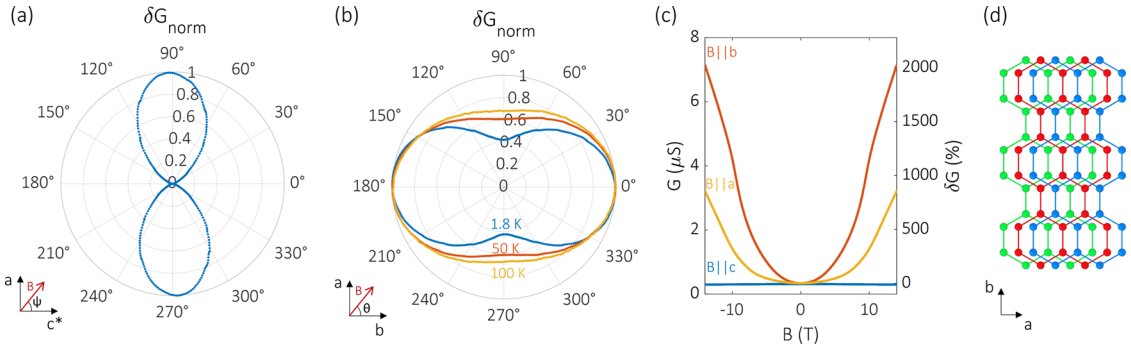

Figure 2. Angle-dependent magnetoconductance of a trilayer α-$RuCl_3$ MTJ. (a) Polar plot of the normalized magnetoconductance δG_{norm} at B = 14 T and T = 1.8 K as a function of ψ in the ac^* plane. (b) Polar plot of the normalized magnetoconductance δG_{norm} at B = 14 T as a function of θ in the ab plane at T = 1.8, 50, and 100 K. (c) Conductance G (left y axis) and magnetoconductance δG (right y axis) as a function of B pointing along the three symmetry axes. These measurements, which were performed by sweeping B in both directions, did not show any sign of hysteretic behavior. All measurements in this figure are performed with V_{app} = 0.4 V. (d) Top view of the stacking order in the monoclinic $C2/m$ phase for the three layers. For simplicity, only the Ru atoms are represented as blue, red, and green spheres, from the top to the bottom layer.

tunneling conductance $G = I/V$ that avoid unwanted contributions from graphite magnetoresistance. The inset of Figure 1b presents an optical image of a typical device comprising a trilayer α-$RuCl_3$ flake. The conductance of every junction decreases in a thermally activated way as the junction is cooled to a temperature T of about 30 K (Figure 1b). The value of this activation energy is almost identical for all junctions, regardless of the α-$RuCl_3$ thickness, with an average of $\phi_0 = 0.26 \pm 0.03$ eV (see Supporting Information, Figure S2). We attribute this behavior to thermionic transport over the potential barrier of height ϕ_0 formed at the graphite/α-$RuCl_3$ interface. This value of ϕ_0 is consistent with a recent scanning tunneling spectroscopy study on few-layer α-$RuCl_3$/graphite which indicates that upper bands are ~0.3 eV above the Fermi level.[29]

At low temperatures, the conductivity shows a weak temperature dependence, indicating that transport across the junction is dominated by electron tunneling. The strongly nonlinear I–V curves measured at T = 1.8 K (Figure 1c) imply that α-$RuCl_3$ flakes behave as insulating barriers. At high bias, the transport can be described by the Fowler–Nordheim (FN) tunneling[49] relation $I \propto \frac{V^2}{\phi_0} e^{\alpha \phi_0^{3/2}/V}$, where $\alpha = \frac{4tN\sqrt{2m^*}}{3\hbar q}$ (see Figure 1d). Here, t = 0.6 nm is the layer thickness of α-$RuCl_3$, N is the number of layers, m^* is the effective mass of carriers along the tunneling direction, $\hbar$ is the reduced Planck constant and q is the elementary charge. The inset of Figure 1d shows a linear relation between $\alpha\phi_0^{3/2}$ and N obtained from the FN fits. Using the value of ϕ_0 deduced from the temperature dependence of G, we estimate the effective mass inside the α-$RuCl_3$ barrier to be $m^* \simeq 9\ m_0$, where m_0 is the free electron mass. This large m^* value reflects the highly correlated nature of electrons and the resulting nondispersive bands in α-$RuCl_3$, as confirmed below by *ab initio* calculations.

Having established that electron tunneling through Mott-insulating α-$RuCl_3$ is the dominant transport mechanism at low temperatures, we investigate the effect of applying an in-plane magnetic field B on the transport properties. Figure 1e shows a large increase in the tunneling current in the trilayer junction, which implies that the tunneling probability is linked to the field-dependent magnetic structure of α-$RuCl_3$. The junction magnetoconductance, which is defined has $\delta G = [G(B, V) - G(0, V)]/G(0, V)$ and plotted in Figure 1f, reaches a peak at finite bias. As observed in other MTJs,[41,48] this peak corresponds to the onset of the FN tunneling regime. As we demonstrate below, the magnetoconductance in this regime can be well described by a spin-dependent tunneling model[40,46,50] where the majority-spin electrons experience a lower energy barrier than that of minority-spin electrons. As a result, our junctions display large (>3000%) magnetoconductance under an in-plane magnetic field of 14 T. This large magnetoconductance provides a sensitive probe to study the magnetic structure of exfoliated α-$RuCl_3$ flakes. Unless otherwise specified, all measurements presented below are obtained from the trilayer device. Other devices exhibit qualitatively similar behavior and are presented in the Supporting Information.

Magnetic Anisotropy. First, we examine the magnetic anisotropy of α-$RuCl_3$ crystals by measuring G as a function of the orientation of B with respect to the c^* axis (angle ψ, Figure 2a) and within the ab plane (angle θ, Figure 2b). While a large increase of the conductance G_{ab} is observed when B lies in the ab plane, only a small decrease of G_{c^*} ($\sim -1\%$) is detected when B is perpendicular to the α-$RuCl_3$ plane (Figure 2c). We attribute this negative δG to the positive magnetoresistance of the graphite contacts.[51] This leads to a giant tunneling anisotropic magnetoresistance effect, TAMR = $(G_{ab} - G_{c^*})/G_{c^*}$, as high as ~2500%. This effect typically arises when electrons are tunneling into a material with large spin–orbit coupling and magnetic anisotropy,[52,53] as is the case here. In α-$RuCl_3$, the spin–orbit coupling leads to an off-diagonal AFM exchange interaction Γ that is comparable in size to the Kitaev interaction.[54−56] This Γ interaction forces the moments to lie in the ac plane with a finite c-axis component, which gives rise to the strong easy-plane magnetic anisotropy observed in bulk crystals[9−11,54,57] and the large out-of-plane TAMR we measure.

The in-plane magnetoconductance also displays significant anisotropy (Figure 2b), resulting in an in-plane TAMR ratio, $(G_b - G_a)/G_a$, of up to ~120% at low temperatures. The 2-fold symmetry of the TAMR is observed over the entire range of the magnetic field (see Figure 2c and Supporting Information, Figure S3). It also survives at a high temperature (T > 100 K), far above the magnetic transition temperature typically observed in α-$RuCl_3$ ($T_N \simeq 7$–14 K). This suggests that this in-plane TAMR does not stem from a long-range magnetic order but rather from the anisotropy of the spin

https://doi.org/10.1021/acsnano.4c06937
ACS Nano XXXX, XXX, XXX−XXX

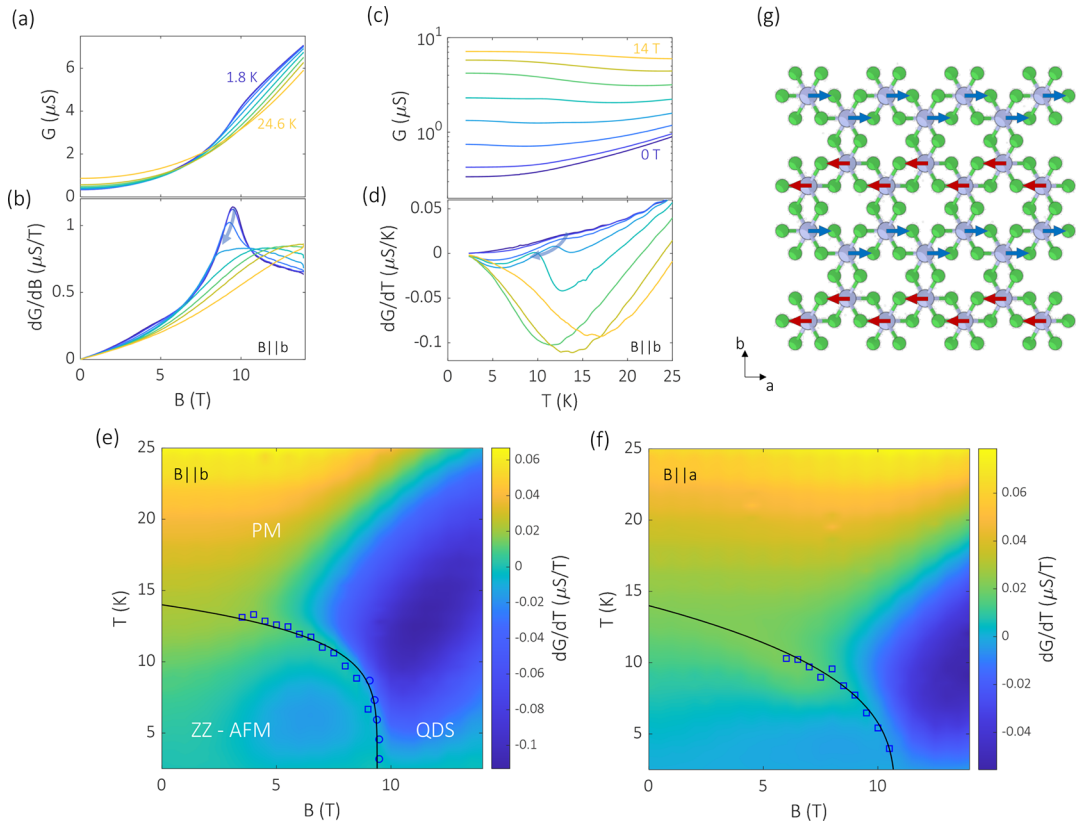

Figure 3. Magnetic phase diagram of trilayer α-$RuCl_3$. (a) Conductance G and its derivative dG/dB (b) as a function of magnetic field B at selected temperatures T between 1.8 and 24.6 K. (c) Conductance G and its derivative dG/dT (d) as a function of T at selected values of B between 0 and 14 T. The arrows in (b) and (d) indicate the position and evolution of peaks in the derivative. (e, f) Color plot of dG/dT as a function of T and B, with B pointing along the b and a axes of the crystal, respectively. Three phases are identified: zigzag antiferromagnetic (ZZ-AFM), paramagnetic (PM) and partially polarized quantum disordered state (QDS). The blue circles and squares correspond to the positions of the peaks in dG/dB and dG/dT, respectively. The black lines are fits to those data points, as described in the main text. All measurements in this figure are performed with V_{app} = 0.4 V. (g) Top view of the crystal and ZZ-AFM spin structure of a α-$RuCl_3$ monolayer. According to ref 63, spins (red and blue arrows) lie in the ac plan. Ru and Cl atoms are represented by gray and green spheres, respectively.

Hamiltonian.[58] These observations contrast with the 6-fold periodicity recently reported for bulk α-$RuCl_3$,[59,60] but they match the 2-fold symmetry of the in-plane susceptibility observed by Lampen−Kelley *et al.*[61] in other bulk samples. The latter demonstrated that this effect is consistent with a monoclinic $C2/m$ crystal structure (Figure 2d), where the a (b) axis corresponds to the direction of the minimum (maximum) susceptibility. Accordingly, in our samples, we ascribe the direction of lower (higher) magnetoconductance to the a (b) axis of the α-$RuCl_3$ flake. We note that the extrema of $\delta G(\theta)$ in the ab plane often coincide with the orientation of one of the crystal edges[62] of the α-$RuCl_3$ flakes (e.g., see the inset of Figure 1b), suggesting that the TAMR is indeed linked to the symmetry of the magnetocrystalline anisotropy. Finally, we point out that similar out-of-plane and in-plane TAMR effects are observed in thicker flakes (see Supporting Information, Figure S4).

Magnetic Phase Diagram. In addition to identifying the magnetocrystalline axes of our α-$RuCl_3$ flakes, magnetoconductance measurements allow us to probe their magnetic phase boundaries. We do so by measuring the conductance G as a function of temperature T and the magnetic field B applied along their a and b axes. Figure 3a shows G as a function of B at selected values of T for $B \| b$. At low temperatures, G exhibits a nearly quadratic field dependence which becomes almost linear when $B > B_c \simeq 9-10$ T. Beyond this critical field, G does not appear to entirely saturate, even up to 14 T. This transition is made more visible by taking the derivative of G with respect to B as shown in Figure 3b. We see that the peak corresponding to the transition shifts toward the lower field and decreases as temperature increases. To further investigate this transition, we consider the temperature dependence of G at selected values of B (Figure 2c) and its derivative dG/dT (Figure 3d). At low field ($B < B_c$), a small peak is observed in dG/dT at a Néel temperature $T_N \sim 14$ K, which shifts to lower temperatures as B increases. In contrast, at a high field ($B > B_c$), a dip appears in dG/dT that moves to higher temperatures with increasing B.

These results can be represented more effectively by plotting the color map of dG/dT as a function of T and B, as illustrated in Figure 3e. This map is strongly reminiscent of a typical magnetic field-temperature phase diagram. We see that the phase boundary coincides well with the position of the peak extracted from the dG/dB and dG/dT curves (open blue circles and squares, respectively). This phase boundary can be fitted using the power law $T_N(B) = T_N(0)(1 - B/B_c)^{\nu z}$, where the exponent $\nu z \simeq 0.16$, $B_c \simeq 9.4$ T and the zero-field Néel temperature $T_N(0) \simeq 14$ K. We also performed similar measurements and analysis with $B \| a$, as shown in Figure 3f. In this case, the phase boundary is best described by the power law parameters $\nu z \simeq 0.33$ and $B_c \simeq 10.7$ T. We note that a

https://doi.org/10.1021/acsnano.4c06937
ACS Nano XXXX, XXX, XXX−XXX

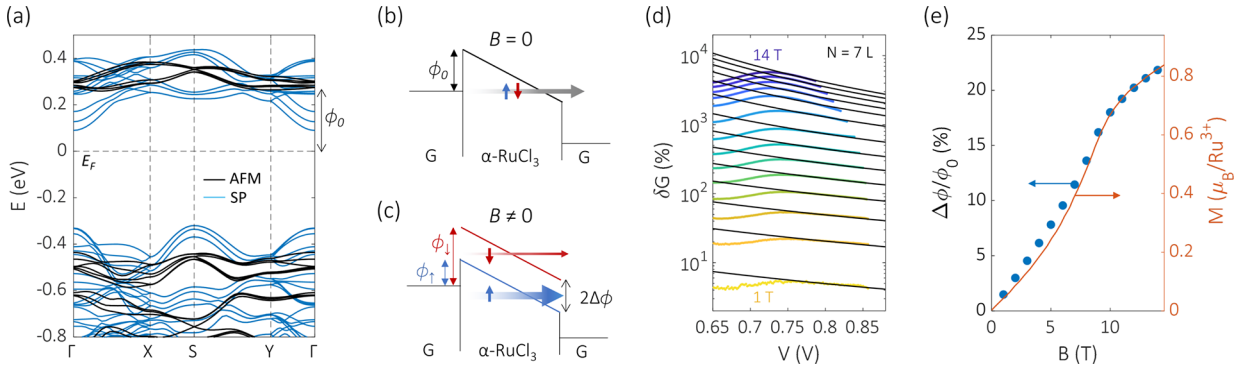

Figure 4. Electronic structure and origin of the magnetoconductance in α-$RuCl_3$. (a) DFT calculations of the band structure of trilayer α-$RuCl_3$ with $C2/m$ stacking with zigzag AFM (black lines) or spin polarized (PS, blue lines) magnetic order. The energy barrier height ϕ_0 between the bottom of the α-$RuCl_3$ upper band and the Fermi energy E_F is indicated. (b, c) Energy band diagrams of graphite/α-$RuCl_3$/graphite tunnel junctions (b) at zero field and (c) under an in-plane magnetic field B. $\phi_{\uparrow,\downarrow}$ represents the energy barrier height experienced by majority- and minority-spin electrons. $2\Delta\phi = \phi_\downarrow - \phi_\uparrow$ is the total spin splitting energy between the two bands. The width of the arrows represents the magnitude of the tunneling current. (d) Magnetoconductance δG as a function of voltage V across a α-$RuCl_3$ flake with $N = 7$ layers at 1.8 K and selected values of B. The black lines are fits to the data using a spin-dependent FN tunneling model. Each fit yields a single fitting parameter, $\Delta\phi$. e Left y axis: $\Delta\phi/\phi_0$ as a function of B (blue dots), where $\Delta\phi$ is obtained from the fits in (d) and $\phi_0 = 0.26$ eV. Right y axis: Magnetization M as a function of in-plane magnetic field B measured on a single crystal of α-$RuCl_3$ with monoclinic $C2/m$ structure (orange line, taken from ref 9.).

similar phase boundary is observed in thicker α-$RuCl_3$ flakes (see Supporting Information, Figure S5).

DISCUSSION

The origin of this phase boundary can be readily interpreted by comparing it to the one observed in bulk α-$RuCl_3$.[9,15,16,59,60] Like in the bulk case, we ascribe the magnetic ground state of our exfoliated flake to a zigzag AFM order (Figure 3g). Indeed, at low field, G exhibits a small drop as T decreases below T_N, which is most visible in thicker flakes (see the Supporting Information, Figure S5). Such kinks are typically observed in MTJs with AFM interlayer order and attributed to a spin filter effect.[39,42,45,48] This suggests that the ground state of α-$RuCl_3$ flakes presents both intra- and interlayer AFM order, in agreement with observations in the bulk.[9,13,63] At the intermediate field, bulk crystals have been found to undergo a field-induced phase transition from this magnetically ordered state to a partially polarized quantum-disordered state (QDS).[9,16,19,64] While the exact nature of this state is still under debate, it is typically characterized by a gapped spin-excitation continuum[64,65] and quantum fluctuations that prevent complete spin alignment. As a result, magnetic saturation can be approached only asymptotically with increasing B. This provides an explanation for the steadily increasing $G(B)$ we observe at high field (Figure 3a), which contrasts with the magnetoconductance plateaus typically observed in other layered transition metal trihalides.[38,39] In this high-field regime, the decrease of G with increasing temperature (Figure 3c) can be interpreted as a reduction of the spin polarization due to enhanced thermal fluctuations, ultimately resulting in a paramagnetic (PM) state. The minimum in dG/dT (Figure 3d) appears to demarcate the crossover between the PM and the gapped QDS states.

Next, we discuss the effect of the in-plane magnetic field orientation on the magnetic phase boundary. As can be seen by comparing Figure 3e,f, B_c is slightly higher for $B\|a$ (perpendicular to the Ru−Ru bonds) than for $B\|b$ (parallel to the Ru−Ru bonds). This is consistent with our observation that $\delta G_b > \delta G_a$, which suggests that the magnetic susceptibility is higher for $B\|b$. In contrast, in many bulk samples, B_c exhibits a 6-fold rotational symmetry and is maximum when the field is parallel to the Ru−Ru bonds.[59,60] However, Mi *et al.* have found that this can be sample-dependent, having observed a maximum B_c perpendicular to the Ru−Ru bonds for one of their bulk samples.[66] It is worth noting that several of these bulk samples exhibit one or several ordered phases below B_c. Some of our magnetoconductance measurements also indicate the presence of an intermediate phase when $B\|a$. It is most visible in devices with thicker flakes, in particular, $N = 7$ layers (see Supporting Information, Figure S5i). This phase might have the same origin as the narrow ZZ2[60] or X[59,66] phase observed in bulk samples (also most prominent for fields perpendicular to the Ru−Ru bonds), in which the magnetic structure adopts a 6-layer stacking, instead of the 3-layer stacking at lower fields.[58−60,62]

In general, we note that the values of T_N and B_c we measure are larger than those typically reported for high-quality bulk samples[12,16,20,59,60] ($T_N \sim 7$ K, $B_c \sim 6$ to 8 T), but similar to those observed in samples with a high density of stacking faults[9,10,57,63,66] ($T_N \sim 14$ K, $B_c \sim 8$ to 10 T). This enhanced T_N has been linked to the two-layer stacking periodicity (ABAB) present in samples in powder form[9,13] or those that have been mechanically deformed.[63] Indeed, owing to the weak van der Waals forces between individual layers, polytypes of α-$RuCl_3$ have very small structural energy differences (<1 meV),[67] making this material prone to stacking disorder. To determine the layer stacking order in our flakes, we performed high-angle annular dark field scanning transmission electron microscopy (HAADF-STEM) on a ∼16 nm-thick exfoliated flake at room temperature (see Supporting Information, Section II). While we predominantly observe STEM images consistent with the $C2/m$ space group, we also observe several alternative structures that are not well-described by the $C2/m$ structure or other known stacking orders of α-$RuCl_3$. Instead, we posit that these regions contain disordered stacking and stacking faults as observed in other exfoliated 2D materials, such as $MoTe_2$[68] and TaS_2.[69] These stacking faults may originate from extrinsic effects such as the strain applied on the flakes during their mechanical exfoliation or from intrinsic

https://doi.org/10.1021/acsnano.4c06937
ACS Nano XXXX, XXX, XXX−XXX

confinement effects on the stacking-dependent free energy.[68] The in-plane stacking domain size is <1 μm, and given that the area of our MTJ is typically on the order of 20 μm^2, we infer that they most certainly contain several stacking configurations.

The presence of stacking faults can have an important effect on the low-temperature crystal structure. Bulk α-$RuCl_3$ typically is believed to undergo a crystallographic phase transition around 150 K from a monoclinic $C2/m$ structure at room temperature to a rhombohedral $R\bar{3}$ structure at low temperature.[57,66,70,71] However, the 2-fold rotational symmetry of our angle-dependent magnetoconductance measurements (Figure 2b) indicates that the structure of our flakes remains in the $C2/m$ phase at low temperatures. Additionally, our temperature-dependent transport measurements (Figure 1b, for example) show no sign of a structural transition, which should manifest as a jump in $G(T)$. A plausible explanation is that the stacking disorder effectively quenches the structural transition by pinning the crystal in the monoclinic phase. Similar effects have been observed in small α-$RuCl_3$ samples[63] and other thin exfoliated flakes.[48,68,72] For α-$RuCl_3$, variation in the stacking structures can affect not only the interlayer coupling but also several of the intralayer interactions such as the Kitaev and Γ interactions.[67] Hence, the larger values of T_N and B_c that we observe likely stem from the frozen-in monoclinic phase of our exfoliated flakes.

Finally, we use this knowledge to gain insight into the microscopic mechanism governing magnetoconductance in our MTJs. For that purpose, we carried out density function theory (DFT) calculations of the band structure of trilayer α-$RuCl_3$ with a $C2/m$ stacking order (see Methods for calculations details). Initial calculations were performed with graphene layers on both sides of α-$RuCl_3$, but they failed to capture the insulating behavior of α-$RuCl_3$ found in our experiment (see Supporting Information, Section III). Since we are interested in understanding the effect of the external field on the α-$RuCl_3$ bands, we computed the band structures of α-$RuCl_3$ without graphene in the zigzag AFM and spin-polarized (SP) magnetic configurations (Figure 4a). In this case, we find that the Fermi energy (E_F) lies in the gap. The upper bands are composed of $J_{eff} = 1/2$ while the lower bands are a combination of $J_{eff} = 1/2$ and 3/2. However, since the precise location of E_F cannot be determined numerically, we impose that it match the experimentally obtained value of ϕ_0, i.e. the energy difference between the bottom of the $J_{eff} = 1/2$ bands and E_F at zero field. In the zero-field AFM configuration, the α-$RuCl_3$ bands are quite flat and lack aclear spin splitting, so electron tunneling is expected to be spin-independent (Figure 4b). In the SP phase, the conduction band is completely spin-polarized, and majority-spin electrons experience a significantly reduced energy barrier. The relative energy shift of the potential barrier ($\Delta\phi/\phi_0$) varies with the momentum, ranging from 15% around the X point to 65% at the Γ point. This magnetically dependent lowering of the energy barrier leads to an exponential increase of the tunneling current, thus explaining, at least qualitatively, the large magnetoconductance that we observe.

We can quantitively compare our experimental results to these DFT calculations by analyzing our measurements with a simple spin-dependent FN tunneling model.[40,46,50] In this phenomenological model, tunneling electrons with spin up and down experience tilted energy barriers with different heights $\phi_{\uparrow,\downarrow}$ (Figure 4c, see Supporting Information, Section IV). We assume, as done by Wang *et al.*,[40] that the field-induced spin splitting $\Delta\phi$ of the conduction band is symmetrical around the zero-field barrier height, i.e., $\phi_{\uparrow,\downarrow} = \phi_0 \pm \Delta\phi(B)$. Figure 4d shows that this simple model captures well the decrease of the magnetoconductance at large bias for different values of B. From each curve, we extract a single fitting parameter, $\Delta\phi(B)$, which we normalized by ϕ_0 in Figure 4e. The maximum relative change extracted at B = 14 T is on the order of 20%, which is comparable to our DFT predictions. Interestingly, the spin splitting energy $\Delta\phi(B)$ follows closely the magnetization curve $M(B)$ measured in bulk α-$RuCl_3$ with a monoclinic structure.[9] This suggests, as previously reported for $CrBr_3$,[40] that the spin-splitting energy is linearly proportional to the magnetization, which elucidates the relation between the tunneling magnetoconductance of α-$RuCl_3$ and its magnetization.

CONCLUSIONS

In summary, our study of α-$RuCl_3$ demonstrates that angle-dependent TMR measurements can provide a multitude of information on the magnetic, electronic, and crystal properties of ultrathin frustrated magnets. We find that they exhibit a strong easy-plane magnetic anisotropy with a 2-fold in-plane symmetry, indicating that their structure remains in the monoclinic phase at low temperatures. As a result, exfoliated flakes present a zigzag AFM magnetic ground state with enhanced critical values (T_N, B_c) compared with bulk α-$RuCl_3$ with rhombohedral stacking. These results demonstrate the influence of stacking order on the magnetic properties of van der Waals materials. This sets the stage for generating exotic magnetic phases, such as QSLs, by controlling the layer stacking via, for instance, hydrostatic pressure[73,74] or twisting.[75] As such, our work can potentially facilitate the development of spintronic devices exploiting emergent excitations in these unconventional phases.

METHODS

Crystal Synthesis. Single-crystal $RuCl_3$ was synthesized from α-$RuCl_3$ powder provided by Furuya Metals (Japan). The powder was sealed in a quartz ampule that had been purged with argon and then placed under vacuum. The ampoule was heated to 1060 °C at 1.6 °C/min. It was held at 1060 °C for 12 h before being slowly cooled to 600 °C at 6 °C/h. Crystals grew via chemical vapor transport as shiny black plates. These were characterized via X-ray diffraction and magnetic susceptibility to determine the phase purity and sample quality. A single peak in the susceptibility was observed around 7 K. This peak, along with the absence of an additional peak around 14 K, has been shown to indicate low stacking fault density.[63]

Device Fabrication and Transport Measurements. α-$RuCl_3$ flakes were mechanically exfoliated from the bulk crystal. Tunnel junctions of hBN/graphite/α-$RuCl_3$/graphite were assembled using a dry pick-up technique using stamps of PDMS/PC. We note that the relative angle between the crystalline axes of the flakes is not controlled. Some of the heterostructures were fabricated inside a glovebox filled with N_2, others in air. No difference was observed in the quality of the junction, which indicates that α-$RuCl_3$ is air-stable. The heterostructures were deposited onto a silicon substrate with a 285 nm oxide layer, and prepatterned Ti/Au allowed for contact with the graphite electrodes. Transport measurements were performed in a cryostat from Quantum Design (Dynacool Physical Properties Measurement System) equipped with a sample rotator. We used a combination of a DC voltage source (Yokogawa GS200), multimeter (Agilent 34410A), and current preamplifier (Ithaco 1211) to measure the conductance of the junction, as well as the graphite flakes. To ensure an accurate measurement of the tunnel junction and avoid the

https://doi.org/10.1021/acsnano.4c06937
ACS Nano XXXX, XXX, XXX−XXX

contribution from its graphite contacts, we verified that the junction resistance was always much greater than that of the graphite flakes.

DFT Calculations. The density functional theory (DFT) calculations are performed with Vienna ab initio Simulation Packages (VASP)[76] with the projector augmented wave potential[77] and the Perdew–Burke–Ernzerhof (PBE)[78] exchange-correlation functionals. Three layers of α-$RuCl_3$ with a $C2/m$ type stacking type (rectangular unit cell) are considered. A vacuum layer of 15 Å is included to avoid interactions between images due to the periodic boundary conditions. The energy cutoff for the plane-wave basis is 400 eV and the k-point mesh is $6 \times 3 \times 1$. Both the spin–orbit coupling (SOC) effect and the onsite effective Coulomb interactions U = 1.5 eV are included.[79] For the zigzag AFM calculations, the magnetic structure has intralayer AFM zigzag chains and is AFM between layers. The magnetic moments are in the ac plane with a small c-axis component. For spin-polarized (SP) calculations, the magnetic moments are along the a-axis.

ASSOCIATED CONTENT

Data Availability Statement

M.M.; S.D.; X.L.; J.L.H.; E.G.; P.L.-K.; J.Y.; D.G.M.; S.E.N.; K.W.; T.T.; B.R.; J.J.C.; H.-Y.K.; J.A.Q. Giant anisotropic magnetoresistance in few-layer α-$RuCl_3$ tunnel junctions. 2024, 2407.19685. arXiv. https://arxiv.org/abs/2407.19685 (accessed August 18, 2024).

Supporting Information

The Supporting Information is available free of charge at https://pubs.acs.org/doi/10.1021/acsnano.4c06937.

Additional measurements on α-$RuCl_3$ tunnel junctions, high angle annular dark field scanning transmission electron microscopy, additional DFT calculations, and spin-dependent Fowler–Nordheim tunneling model (PDF)

AUTHOR INFORMATION

Corresponding Author

Mathieu Massicotte – *Institut quantique and Département de physique, Université de Sherbrooke, Sherbrooke, QC J1K 2R1, Canada; Institut Interdisciplinaire d'Innovation Technologique (3iT), Laboratoire Nanotechnologies Nanosystèmes (LN2) - CNRS IRL-3463 and Département de génie électrique et génie informatique, Université de Sherbrooke, Sherbrooke J1K 2R1, Canada;* orcid.org/0000-0003-2802-2829; Email: mathieu.massicotte@usherbrooke.ca

Authors

Sam Dehlavi – *Institut quantique and Département de physique, Université de Sherbrooke, Sherbrooke, QC J1K 2R1, Canada*

Xiaoyu Liu – *Department of Physics, University of Toronto, Toronto, Ontario M5S 1A7, Canada*

James L. Hart – *Department of Materials Science and Engineering, Cornell University, Ithaca, New York 14853, United States*

Elio Garnaoui – *Institut quantique and Département de physique, Université de Sherbrooke, Sherbrooke, QC J1K 2R1, Canada*

Paula Lampen-Kelley – *Department of Materials Science and Engineering, University of Tennessee, Knoxville, Tennessee 37996, United States; Materials Science and Technology Division, Oak Ridge National Laboratory, Oak Ridge, Tennessee 37831, United States*

Jiaqiang Yan – *Department of Materials Science and Engineering, University of Tennessee, Knoxville, Tennessee 37996, United States; Materials Science and Technology Division, Oak Ridge National Laboratory, Oak Ridge, Tennessee 37831, United States;* orcid.org/0000-0001-6625-4706

David G. Mandrus – *Department of Materials Science and Engineering, University of Tennessee, Knoxville, Tennessee 37996, United States; Materials Science and Technology Division, Oak Ridge National Laboratory, Oak Ridge, Tennessee 37831, United States;* orcid.org/0000-0003-3616-7104

Stephen E. Nagler – *Department of Physics and Astronomy, University of Tennessee, Knoxville, Tennessee 37996, United States; Neutron Scattering Division, Oak Ridge National Laboratory, Oak Ridge, Tennessee 37831, United States*

Kenji Watanabe – *National Institute for Materials Science, Tsukuba 305-0044, Japan*

Takashi Taniguchi – *National Institute for Materials Science, Tsukuba 305-0044, Japan;* orcid.org/0000-0002-1467-3105

Bertrand Reulet – *Institut quantique and Département de physique, Université de Sherbrooke, Sherbrooke, QC J1K 2R1, Canada*

Judy J. Cha – *Department of Materials Science and Engineering, Cornell University, Ithaca, New York 14853, United States;* orcid.org/0000-0002-6346-2814

Hae-Young Kee – *Department of Physics, University of Toronto, Toronto, Ontario M5S 1A7, Canada*

Jeffrey A. Quilliam – *Institut quantique and Département de physique, Université de Sherbrooke, Sherbrooke, QC J1K 2R1, Canada*

Complete contact information is available at: https://pubs.acs.org/10.1021/acsnano.4c06937

Notes

The authors declare no competing financial interest.

ACKNOWLEDGMENTS

X.L. and H.Y.K. acknowledge the support of the Natural Sciences and Engineering Research Council of Canada (Discovery Grants No. RGPIN2022-04601). H.Y.K. also acknowledges the support of the Canadian Institute for Advanced Research and the Canada Research Chairs Program. J.L.H. and J.J.C. acknowledge generous support from the Gordon and Betty Moore Foundation under the EPiQS program, GBMF9062.01. The microscopy facilities at Cornell are supported through the NSF MRSEC program (DMR-1719875). S.E.N. and J.Q.Y. were supported by the U.S. Department of Energy, Office of Science, National Quantum Information Science Research Centers, Quantum Science Center; this support contributed to the growth and characterization of the crystals used in this work. D.G.M. acknowledges support from the Gordon and Betty Moore Foundation's EPiQS Initiative, Grant GBMF9069. M.M., J.A.Q., and B.R. acknowledge research funding from the Canada First Research Excellence Fund and the Natural Sciences and Engineering Research Council of Canada. B.R. also acknowledges support from the Canada Research Chair program, the Canada Foundation for Innovation, and the FRQNT. Finally, M.M. acknowledges support from the support of the Natural Sciences and Engineering Research Council of Canada

(Discovery Grants No. RGPIN-2023-04764). We thank Gabriel Laliberté, Christian Lupien, and Jordan Baglo for technical support, and acknowledge helpful discussions with Quentin Barthélemy and Alessandro Principi.

REFERENCES

(1) Savary, L.; Balents, L. Quantum spin liquids: a review. *Rep. Prog. Phys.* **2017**, *80*, No. 016502.
(2) Anderson, P. W. Resonating valence bonds: A new kind of insulator? *Mater. Res. Bull.* **1973**, *8*, 153−160.
(3) Balents, L. Spin liquids in frustrated magnets. *Nature* **2010**, *464*, 199−208.
(4) Kitaev, A. Anyons in an exactly solved model and beyond. *Annals of Physics* **2006**, *321*, 2−111.
(5) Nayak, C.; Simon, S. H.; Stern, A.; Freedman, M.; Das Sarma, S. Non-Abelian anyons and topological quantum computation. *Rev. Mod. Phys.* **2008**, *80*, 1083−1159.
(6) Jackeli, G.; Khaliullin, G. Mott Insulators in the Strong Spin-Orbit Coupling Limit: From Heisenberg to a Quantum Compass and Kitaev Models. *Phys. Rev. Lett.* **2009**, *102*, No. 017205.
(7) Takagi, H.; Takayama, T.; Jackeli, G.; Khaliullin, G.; Nagler, S. E. Concept and realization of Kitaev quantum spin liquids. *Nature Reviews Physics* **2019**, *1*, 264−280.
(8) Plumb, K. W.; Clancy, J. P.; Sandilands, L. J.; Shankar, V. V.; Hu, Y. F.; Burch, K. S.; Kee, H.-Y.; Kim, Y.-J. α-$RuCl_3$: A spin-orbit assisted Mott insulator on a honeycomb lattice. *Phys. Rev. B* **2014**, *90*, No. 041112.
(9) Johnson, R. D.; Williams, S. C.; Haghighirad, A. A.; Singleton, J.; Zapf, V.; Manuel, P.; Mazin, I. I.; Li, Y.; Jeschke, H. O.; Valentí, R.; Coldea, R. Monoclinic crystal structure of α-$RuCl_3$ and the zigzag antiferromagnetic ground state. *Phys. Rev. B* **2015**, *92*, No. 235119.
(10) Sears, J. A.; Songvilay, M.; Plumb, K. W.; Clancy, J. P.; Qiu, Y.; Zhao, Y.; Parshall, D.; Kim, Y. J. Magnetic order in α-$RuCl_3$: A honeycomb-lattice quantum magnet with strong spin-orbit coupling. *Phys. Rev. B* **2015**, *91*, No. 144420.
(11) Majumder, M.; Schmidt, M.; Rosner, H.; Tsirlin, A. A.; Yasuoka, H.; Baenitz, M. Anisotropic Ru3+ 4d5 magnetisminthe α-$RuCl_3$ honeycomb system: Susceptibility, specific heat, and zero-field NMR. *Phys. Rev. B* **2015**, *91*, No. 180401.
(12) Banerjee, A.; Yan, J.; Knolle, J.; Bridges, C. A.; Stone, M. B.; Lumsden, M. D.; Mandrus, D. G.; Tennant, D. A.; Moessner, R.; Nagler, S. E. Neutron scattering in the proximate quantum spin liquid α-$RuCl_3$. *Science* **2017**, *356*, 1055−1059.
(13) Banerjee, A.; et al. Proximate Kitaev quantum spin liquid behaviour in a honeycomb magnet. *Nat. Mater.* **2016**, *15*, 733−740.
(14) Nasu, J.; Knolle, J.; Kovrizhin, D. L.; Motome, Y.; Moessner, R. Fermionic response from fractionalization in an insulating two-dimensional magnet. *Nat. Phys.* **2016**, *12*, 912−915.
(15) Zheng, J.; Ran, K.; Li, T.; Wang, J.; Wang, P.; Liu, B.; Liu, Z.-X.; Normand, B.; Wen, J.; Yu, W. Gapless Spin Excitations in the Field-Induced Quantum Spin Liquid Phase of α-$RuCl_3$. *Phys. Rev. Lett.* **2017**, *119*, No. 227208.
(16) Sears, J. A.; Zhao, Y.; Xu, Z.; Lynn, J. W.; Kim, Y. J. Phase diagram of α-$RuCl_3$ in an in-plane magnetic field. *Phys. Rev. B* **2017**, *95*, No. 180411.
(17) Wolter, A. U.; Corredor, L. T.; Janssen, L.; Nenkov, K.; Schönecker, S.; Do, S. H.; Choi, K. Y.; Albrecht, R.; Hunger, J.; Doert, T.; Vojta, M.; Büchner, B. Field-induced quantum criticality in the Kitaev system α-$RuCl_3$. *Phys. Rev. B* **2017**, *96*, No. 041405.
(18) Wang, Z.; Reschke, S.; Hüvonen, D.; Do, S. H.; Choi, K. Y.; Gensch, M.; Nagel, U.; Rõõm, T.; Loidl, A. Magnetic Excitations and Continuum of a Possibly Field-Induced Quantum Spin Liquid in α-$RuCl_3$. *Phys. Rev. Lett.* **2017**, *119*, No. 227202.
(19) Baek, S. H.; Do, S. H.; Choi, K. Y.; Kwon, Y. S.; Wolter, A. U.; Nishimoto, S.; Van Den Brink, J.; Böchner, B. Evidence for a field-induced quantum spin liquid in α-$RuCl_3$. *Phys. Rev. Lett.* **2017**, *119*, No. 037201.
(20) Kasahara, Y.; Ohnishi, T.; Mizukami, Y.; Tanaka, O.; Ma, S.; Sugii, K.; Kurita, N.; Tanaka, H.; Nasu, J.; Motome, Y.; Shibauchi, T.; Matsuda, Y. Majorana quantization and half-integer thermal quantum Hall effect in a Kitaev spin liquid. *Nature* **2018**, *559*, 227−231.
(21) Kim, S.; Yuan, B.; Kim, Y. J. α-$RuCl_3$ and other Kitaev materials. *APL Mater.* **2022**, *10*, No. 080903.
(22) Yamashita, M.; Gouchi, J.; Uwatoko, Y.; Kurita, N.; Tanaka, H. Sample dependence of half-integer quantized thermal Hall effect in the Kitaev spin-liquid candidate α-$RuCl_3$. *Phys. Rev. B* **2020**, *102*, No. 220404.
(23) Lefrançois, E.; Grissonnanche, G.; Baglo, J.; Lampen-Kelley, P.; Yan, J. Q.; Balz, C.; Mandrus, D.; Nagler, S. E.; Kim, S.; Kim, Y. J.; Doiron-Leyraud, N.; Taillefer, L. Evidence of a Phonon Hall Effect in the Kitaev Spin Liquid Candidate α-$RuCl_3$. *Physical Review X* **2022**, *12*, No. 021025.
(24) Du, L.; Huang, Y.; Wang, Y.; Wang, Q.; Yang, R.; Tang, J.; Liao, M.; Shi, D.; Shi, Y.; Zhou, X.; Zhang, Q.; Zhang, G. 2D proximate quantum spin liquid state in atomic-thin α-$RuCl_3$. *2D Materials* **2019**, *6*, No. 015014.
(25) Lin, D.; Ran, K.; Zheng, H.; Xu, J.; Gao, L.; Wen, J.; Yu, S. L.; Li, J. X.; Xi, X. Anisotropic scattering continuum induced by crystal symmetry reduction in atomically thin α-$RuCl_3$. *Phys. Rev. B* **2020**, *101*, No. 045419.
(26) Zhou, B.; Wang, Y.; Osterhoudt, G. B.; Lampen-Kelley, P.; Mandrus, D.; He, R.; Burch, K. S.; Henriksen, E. A. Possible structural transformation and enhanced magnetic fluctuations in exfoliated α-$RuCl_3$. *J. Phys. Chem. Solids* **2019**, *128*, 291−295.
(27) Dai, Z.; Yu, J. X.; Zhou, B.; Tenney, A. S.; Lampen-Kelley, P.; Yan, J.; Mandrus, D.; Henriksen, A. E.; Zang, J.; Pohl, K.; Sadowski, J. T. Crystal structure reconstruction in the surface monolayer of the quantum spin liquid candidate α-$RuCl_3$. *2D Mater.* **2020**, *7*, No. 035004.
(28) Vatansever, E.; Sarikurt, S.; Ersan, F.; Kadioglu, Y.; Üzengi Aktürk, O.; Yüksel, Y.; Ataca, C.; Aktürk, E.; Aklncl, U. Strain effects on electronic and magnetic properties of the monolayer α-$RuCl_3$: A first-principles and Monte Carlo study. *J. Appl. Phys.* **2019**, *125*, No. 083903.
(29) Zheng, X.; Jia, K.; Ren, J.; Yang, C.; Wu, X.; Shi, Y.; Tanigaki, K.; Du, R. R. Tunneling spectroscopic signatures of charge doping and associated Mott transition in α-$RuCl_3$ in proximity to graphite. *Phys. Rev. B* **2023**, *107*, No. 195107.
(30) Yang, B.; et al. Magnetic anisotropy reversal driven by structural symmetry-breaking in monolayer α-$RuCl_3$. *Nat. Mater.* **2023**, *22*, 50−57.
(31) Wang, Y.; et al. Modulation Doping via a Two-Dimensional Atomic Crystalline Acceptor. *Nano Lett.* **2020**, *20*, 8446−8452.
(32) Mashhadi, S.; Kim, Y.; Kim, J.; Weber, D.; Taniguchi, T.; Watanabe, K.; Park, N.; Lotsch, B.; Smet, J. H.; Burghard, M.; Kern, K. Spin-Split Band Hybridization in Graphene Proximitized with α-$RuCl_3$ Nanosheets. *Nano Lett.* **2019**, *19*, 4659−4665.
(33) Rizzo, D. J.; et al. Charge-Transfer Plasmon Polaritons at Graphene/α -$RuCl_3$ Interfaces. *Nano Lett.* **2020**, *20*, 8438−8445.
(34) Zhou, B.; Balgley, J.; Lampen-Kelley, P.; Yan, J.-Q.; Mandrus, D. G.; Henriksen, E. A. Evidence for charge transfer and proximate magnetism in graphene−α -$RuCl_3$ heterostructures. *Phys. Rev. B* **2019**, *100*, No. 165426.
(35) Souza, P. H.; Deus, D. P. A.; Brito, W. H.; Miwa, R. H. Magnetic anisotropy energies and metal-insulator transitions in monolayers of α-$RuCl_3$ and $OsCl_3$ on graphene. *Phys. Rev. B* **2022**, *106*, No. 155118.
(36) Biswas, S.; Li, Y.; Winter, S. M.; Knolle, J.; Valentí, R. Electronic Properties of α-$RuCl_3$ in Proximity to Graphene. *Phys. Rev. Lett.* **2019**, *123*, No. 237201.
(37) Gerber, E.; Yao, Y.; Arias, T. A.; Kim, E. A. Ab Initio Mismatched Interface Theory of Graphene on α-$RuCl_3$: Doping and Magnetism. *Phys. Rev. Lett.* **2020**, *124*, No. 106804.
(38) Wang, Z.; Gibertini, M.; Dumcenco, D.; Taniguchi, T.; Watanabe, K.; Giannini, E.; Morpurgo, A. F. Determining the phase

https://doi.org/10.1021/acsnano.4c06937
ACS Nano XXXX, XXX, XXX−XXX

diagram of atomically thin layered antiferromagnet $CrCl_3$. *Nat. Nanotechnol.* **2019**, *14*, 1116−1122.
(39) Klein, D. R.; MacNeill, D.; Lado, J. L.; Soriano, D.; Navarro-Moratalla, E.; Watanabe, K.; Taniguchi, T.; Manni, S.; Canfield, P.; Fernández-Rossier, J.; Jarillo-Herrero, P. Probing magnetism in 2D van der Waals crystalline insulators via electron tunneling. *Science* **2018**, *360*, 1218−1222.
(40) Wang, Z.; Gutiérrez-Lezama, I.; Dumcenco, D.; Ubrig, N.; Taniguchi, T.; Watanabe, K.; Giannini, E.; Gibertini, M.; Morpurgo, A. F. Magnetization dependent tunneling conductance of ferromagnetic barriers. *Nat. Commun.* **2021**, *12*, 6659.
(41) Song, T.; Cai, X.; Tu, M. W. Y.; Zhang, X.; Huang, B.; Wilson, N. P.; Seyler, K. L.; Zhu, L.; Taniguchi, T.; Watanabe, K.; McGuire, M. A.; Cobden, D. H.; Xiao, D.; Yao, W.; Xu, X. Giant tunneling magnetoresistance in spin-filter van der Waals heterostructures. *Science* **2018**, *360*, 1214−1218.
(42) Wang, Z.; Gutiérrez-Lezama, I.; Ubrig, N.; Kroner, M.; Gibertini, M.; Taniguchi, T.; Watanabe, K.; Imamoğlu, A.; Giannini, E.; Morpurgo, A. F. Very large tunneling magnetoresistance in layered magnetic semiconductor CrI_3. *Nat. Commun.* **2018**, *9*, 2516.
(43) Cai, X.; Song, T.; Wilson, N. P.; Clark, G.; He, M.; Zhang, X.; Taniguchi, T.; Watanabe, K.; Yao, W.; Xiao, D.; McGuire, M. A.; Cobden, D. H.; Xu, X. Atomically Thin $CrCl_3$: An In-Plane Layered Antiferromagnetic Insulator. *Nano Lett.* **2019**, *19*, 3993−3998.
(44) Long, G.; Henck, H.; Gibertini, M.; Dumcenco, D.; Wang, Z.; Taniguchi, T.; Watanabe, K.; Giannini, E.; Morpurgo, A. F. Persistence of Magnetism in Atomically Thin $MnPS_3$ Crystals. *Nano Lett.* **2020**, *20*, 2452−2459.
(45) Kim, H. H.; et al. Evolution of interlayer and intralayer magnetism in three atomically thin chromium trihalides. *Proc. Natl. Acad. Sci. U. S. A.* **2019**, *166*, 11131−11136.
(46) Kim, H. H.; Yang, B.; Patel, T.; Sfigakis, F.; Li, C.; Tian, S.; Lei, H.; Tsen, A. W. One Million Percent Tunnel Magnetoresistance in a Magnetic van der Waals Heterostructure. *Nano Lett.* **2018**, *18*, 4885−4890.
(47) Kim, H. H.; Yang, B.; Tian, S.; Li, C.; Miao, G. X.; Lei, H.; Tsen, A. W. Tailored Tunnel Magnetoresistance Response in Three Ultrathin Chromium Trihalides. *Nano Lett.* **2019**, *19*, 5739−5745.
(48) Klein, D. R.; MacNeill, D.; Song, Q.; Larson, D. T.; Fang, S.; Xu, M.; Ribeiro, R. A.; Canfield, P. C.; Kaxiras, E.; Comin, R.; Jarillo-Herrero, P. Enhancement of interlayer exchange in an ultrathin two-dimensional magnet. *Nat. Phys.* **2019**, *15*, 1255−1260.
(49) Simmons, J. G. Generalized Formula for the Electric Tunnel Effect between Similar Electrodes Separated by a Thin Insulating Film. *J. Appl. Phys.* **1963**, *34*, 1793−1803.
(50) Esaki, L.; Stiles, P. J.; von Molnar, S. Magnetointernal field emission in junctions of magnetic insulators. *Phys. Rev. Lett.* **1967**, *19*, 852−854.
(51) Gopinadhan, K.; Shin, Y. J.; Jalil, R.; Venkatesan, T.; Geim, A. K.; Neto, A. H.; Yang, H. Extremely large magnetoresistance in few-layer graphene/boron-nitride heterostructures. *Nat. Commun.* **2015**, *6*, 8337.
(52) Matos-Abiague, A.; Fabian, J. Anisotropic tunneling magnetoresistance and tunneling anisotropic magnetoresistance: Spin-orbit coupling in magnetic tunnel junctions. *Phys. Rev. B* **2009**, *79*, No. 155303.
(53) Tang, H.-M.; Wang, S.-Z.; Jia, X.-T. Tunneling anisotropic magnetoresistance in MgO-based magnetic tunnel junctions induced by spin-orbit coupling. *Phys. Rev. B* **2022**, *106*, No. 094406.
(54) Sears, J. A.; Chern, L. E.; Kim, S.; Bereciartua, P. J.; Francoual, S.; Kim, Y. B.; Kim, Y. J. Ferromagnetic Kitaev interaction and the origin of large magnetic anisotropy in α-$RuCl_3$. *Nat. Phys.* **2020**, *16*, 837−840.
(55) Rau, J. G.; Lee, E. K.-H.; Kee, H.-Y. Generic Spin Model for the Honeycomb Iridates beyond the Kitaev Limit. *Phys. Rev. Lett.* **2014**, *112*, No. 077204.
(56) Chaloupka, J.; Khaliullin, G. Magnetic anisotropy in the Kitaev model systems Na_2IrO_3 and $RuCl_3$. *Phys. Rev. B* **2016**, *94*, No. 064435.
(57) Kubota, Y.; Tanaka, H.; Ono, T.; Narumi, Y.; Kindo, K. Successive magnetic phase transitions in α-$RuCl_3$: XY-like frustrated magnet on the honeycomb lattice. *Phys. Rev. B* **2015**, *91*, No. 094422.
(58) Cen, J.; Kee, H.-Y. Strategy to extract Kitaev interaction using symmetry in honeycomb Mott insulators. *Commun. Phys.* **2022**, *5*, 119.
(59) Tanaka, O.; Mizukami, Y.; Harasawa, R.; Hashimoto, K.; Hwang, K.; Kurita, N.; Tanaka, H.; Fujimoto, S.; Matsuda, Y.; Moon, E. G.; Shibauchi, T. Thermodynamic evidence for a field-angle-dependent Majorana gap in a Kitaev spin liquid. *Nat. Phys.* **2022**, *18*, 429−435.
(60) Balz, C.; Janssen, L.; Lampen-Kelley, P.; Banerjee, A.; Liu, Y. H.; Yan, J. Q.; Mandrus, D. G.; Vojta, M.; Nagler, S. E. Field-induced intermediate ordered phase and anisotropic interlayer interactions in α-$RuCl_3$. *Phys. Rev. B* **2021**, *103*, No. 174417.
(61) Lampen-Kelley, P.; Rachel, S.; Reuther, J.; Yan, J. Q.; Banerjee, A.; Bridges, C. A.; Cao, H. B.; Nagler, S. E.; Mandrus, D. Anisotropic susceptibilities in the honeycomb Kitaev system α-$RuCl_3$. *Phys. Rev. B* **2018**, *98*, No. 100403.
(62) Guo, Y.; Liu, C.; Yin, Q.; Wei, C.; Lin, S.; Hoffman, T. B.; Zhao, Y.; Edgar, J. H.; Chen, Q.; Lau, S. P.; Dai, J.; Yao, H.; Wong, H. S.; Chai, Y. Distinctive in-Plane Cleavage Behaviors of Two-Dimensional Layered Materials. *ACS Nano* **2016**, *10*, 8980−8988.
(63) Cao, H. B.; Banerjee, A.; Yan, J. Q.; Bridges, C. A.; Lumsden, M. D.; Mandrus, D. G.; Tennant, D. A.; Chakoumakos, B. C.; Nagler, S. E. Low-temperature crystal and magnetic structure of α-$RuCl_3$. *Phys. Rev. B* **2016**, *93*, No. 134423.
(64) Sahasrabudhe, A.; et al. High-field quantum disordered state in α-$RuCl_3$: Spin flips, bound states, and multiparticle continuum. *Phys. Rev. B* **2020**, *101*, No. 140410.
(65) Ponomaryov, A. N.; Zviagina, L.; Wosnitza, J.; Lampen-Kelley, P.; Banerjee, A.; Yan, J. Q.; Bridges, C. A.; Mandrus, D. G.; Nagler, S. E.; Zvyagin, S. A. Nature of Magnetic Excitations in the High-Field Phase of α-$RuCl_3$. *Phys. Rev. Lett.* **2020**, *125*, No. 037202.
(66) Mi, X.; Wang, X.; Gui, H.; Pi, M.; Zheng, T.; Yang, K.; Gan, Y.; Wang, P.; Li, A.; Wang, A.; Zhang, L.; Su, Y.; Chai, Y.; He, M. Stacking faults in α-$RuCl_3$ revealed by local electric polarization. *Phys. Rev. B* **2021**, *103*, No. 174413.
(67) Kim, H. S.; Kee, H. Y. Crystal structure and magnetism in α-$RuCl_3$: An ab initio study. *Phys. Rev. B* **2016**, *93*, No. 155143.
(68) Hart, J. L.; et al. Emergent layer stacking arrangements in c-axis confined $MoTe_2$. *Nat. Commun.* **2023**, *14*, 4803.
(69) Hovden, R.; Tsen, A. W.; Liu, P.; Savitzky, B. H.; El Baggari, I.; Liu, Y.; Lu, W.; Sun, Y.; Kim, P.; Pasupathy, A. N.; Kourkoutis, L. F. Atomic lattice disorder in charge-density-wave phases of exfoliated dichalcogenides (1T-TaS_2). *Proc. Natl. Acad. Sci. U.S.A.* **2016**, *113*, 11420−11424.
(70) Reschke, S.; Mayr, F.; Wang, Z.; Do, S. H.; Choi, K. Y.; Loidl, A. Electronic and phonon excitations in α-$RuCl_3$. *Phys. Rev. B* **2017**, *96*, No. 165120.
(71) Glamazda, A.; Lemmens, P.; Do, S. H.; Kwon, Y. S.; Choi, K. Y. Relation between Kitaev magnetism and structure in α-RuCl 3. *Phys. Rev. B* **2017**, *95*, No. 174429.
(72) He, R.; Zhong, S.; Kim, H. H.; Ye, G.; Ye, Z.; Winford, L.; McHaffie, D.; Rilak, I.; Chen, F.; Luo, X.; Sun, Y.; Tsen, A. W. Dimensionality-driven orthorhombic $MoTe_2$ at room temperature. *Phys. Rev. B* **2018**, *97*, No. 041410.
(73) Li, T.; Jiang, S.; Sivadas, N.; Wang, Z.; Xu, Y.; Weber, D.; Goldberger, J. E.; Watanabe, K.; Taniguchi, T.; Fennie, C. J.; Fai Mak, K.; Shan, J. Pressure-controlled interlayer magnetism in atomically thin CrI_3. *Nat. Mater.* **2019**, *18*, 1303−1308.
(74) Song, T.; et al. Switching 2D magnetic states via pressure tuning of layer stacking. *Nat. Mater.* **2019**, *18*, 1298−1302.
(75) Song, T.; Sun, Q. C.; Anderson, E.; Wang, C.; Qian, J.; Taniguchi, T.; Watanabe, K.; McGuire, M. A.; Stöhr, R.; Xiao, D.; Cao, T.; Wrachtrup, J.; Xu, X. Direct visualization of magnetic domains and moiré magnetism in twisted 2D magnets. *Science* **2021**, *374*, 1140−1144.

https://doi.org/10.1021/acsnano.4c06937
ACS Nano XXXX, XXX, XXX−XXX

(76) Kresse, G.; Hafner, J. Ab initio molecular dynamics for liquid metals. *Phys. Rev. B* **1993**, *47*, 558−561.
(77) Blöchl, P. E. Projector augmented-wave method. *Phys. Rev. B* **1994**, *50*, 17953−17979.
(78) Perdew, J. P.; Burke, K.; Ernzerhof, M. Generalized Gradient Approximation Made Simple. *Phys. Rev. Lett.* **1996**, *77*, 3865−3868.
(79) Kim, H.-S.; Vijay Shankar, V.; Catuneanu, A.; Kee, H.-Y. Kitaev magnetism in honeycomb $RuCl_3$ with intermediate spin-orbit coupling. *Phys. Rev. B* **2015**, *91*, No. 241110.

https://doi.org/10.1021/acsnano.4c06937
ACS Nano XXXX, XXX, XXX−XXX